analytical chemistry

Article

Cite This: *Anal. Chem.* 2020, 92, 1379−1385

pubs.acs.org/ac

Anodic Electrochemiluminescence of Carbon Dots Promoted by Nitrogen Doping and Application to Rapid Cancer Cell Detection

Anyi Chen, Wenbin Liang, Haijun Wang, Ying Zhuo, Yaqin Chai,* and Ruo Yuan*

Key Laboratory of Luminescent and Real-Time Analytical Chemistry (Southwest University), Ministry of Education, College of Chemistry and Chemical Engineering, Southwest University, Chongqing 400715, China

Supporting Information

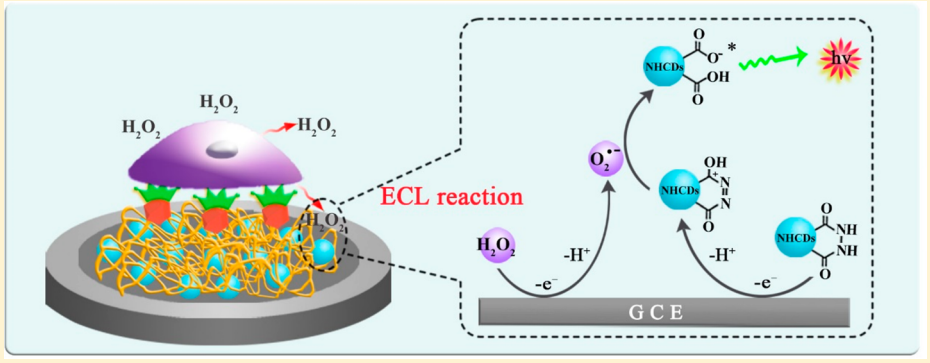

ABSTRACT: In this work, a kind of novel nitrogen doped hydrazide conjugated carbon dots (NHCDs) with strong anodic electrochemiluminescence (ECL) at a low excitation potential were synthesized via a one-step solvothermal approach and applied to construct biosensor for rapid cancer cell detection. The nitrogen doping induced a shift of the highest occupied molecular orbital (HOMO) to the upper energy level thus lowered the anodic ECL excitation potential of carbon dots. Especially, comparing to nondoped hydrazide conjugated carbon dots, NHCDs exhibited 2.5-fold high ECL quantum efficiency because the lower potential could reduce notably the side reactions in the ECL process. Using the high-performance NHCDs to functionalize the electrode surface, a brief ECL biosensor was fabricated to detect the cell-secreted hydrogen peroxide, which could rapidly distinguish cancer cells from normal cells. What is more, the prepared NHCDs, as the combination of low excitation potential, strong ECL emission, and good biocompatibility, were expected to be popular luminophors for clinical diagnose of cancer and monitoring the pharmacodynamics of anticancer drugs.

Electrochemiluminescence (ECL) has attracted increasing research attention[1−5] as it incorporates the outstanding advantages of high sensitivity and good controllability. Conventional applications of ECL methodology in bioanalysis are mainly in vitro detection of biomolecules including nucleic acids,[6] proteins,[7−9] and some small biological molecules.[10,11] In the meantime, ruthenium(II) polypyridyl complexes, benefiting from their strong ECL emission, have been the most widely used luminophors in clinical and research applications.[12,13] However, recent development of ECL methodology has been applied to the analysis of living cells,[14−17] where the significant cytotoxicity of ruthenium(II) polypyridyl complexes[18,19] could seriously interfere the activity of living cells thus reduce the accuracy of result. In this sense, the biocompatibility of ECL systems attracted much attention for the development of in vivo ECL methodology. Therefore, increasing research interest was given to the seeking of new biocompatible ECL luminophors for the alternative of ruthenium(II) polypyridyl complexes.[20,21]

Carbon quantum dots or carbon dots (CDs, including graphene quantum dots) are an emergent class of carbon nanomaterials with attractive luminescent properties,[22−24] which hold promise for widespread applications in bioanalysis benefiting from their outstanding merits in terms of accessibility, stability, and biocompatibility. Since their ECL phenomenon was first reported in 2009,[25] CDs have been promoted as a rising star in ECL luminophors.[26−29] Nevertheless, conventional CDs presented quite weak ECL emission and required high excitation potential, which limited the sensitivity and increased the injury to biological systems. Consequently, improving ECL emission and lowering excitation potential became the primary goal for the practical application of CDs in ECL bioassays. In general, doping nitrogen atoms into the graphitic cores of CDs was the most used strategy to improve the cathodic ECL performance.[30−32] However, the excitation potential of these nitrogen doped CDs presented no observable decrease than that of nondoped CDs in spite of the outstanding improvement in ECL emission, as nitrogen doping could hardly lower the reduction potential of

Received: October 5, 2019
Accepted: November 26, 2019
Published: November 26, 2019

DOI: 10.1021/acs.analchem.9b04537
Anal. Chem. 2020, 92, 1379−1385

Scheme 1. Schematic Illustration of (A) Synthesis Protocol and Structural Model of NHCDs; (B) Principle of the ECL Biosensor for Cancer Cell Detection

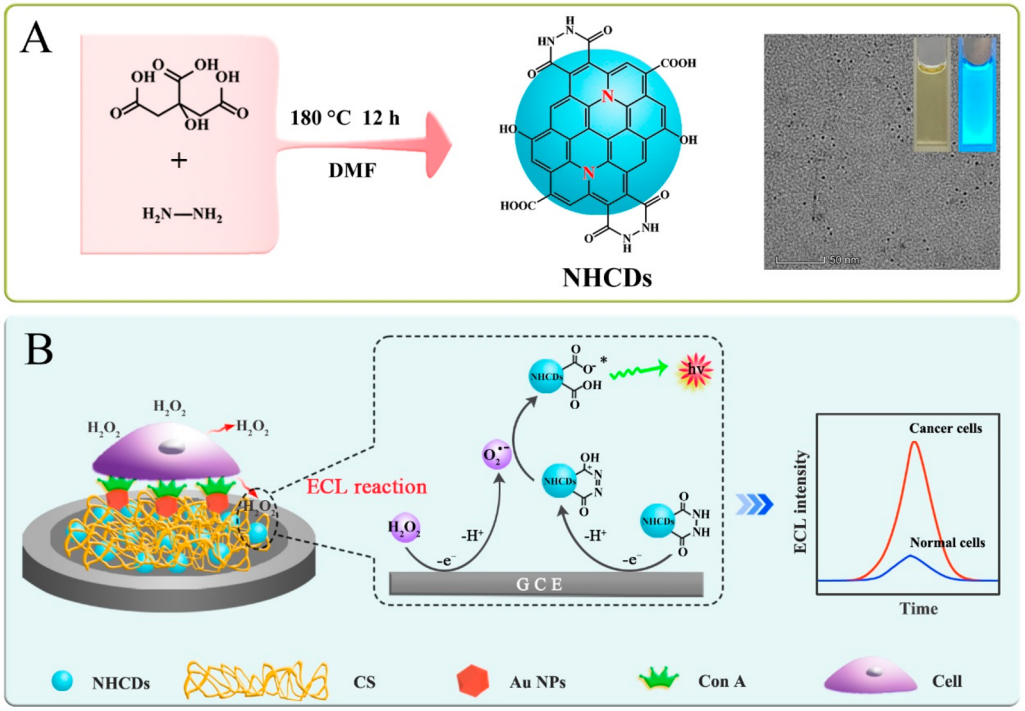

CDs. There emerged an enormous challenge to simultaneously lower excitation and improve ECL emission of CDs. Fortunately, recent evidence showed that nitrogen doping could notably lower the oxidation potential of carbon nanomaterials.[33,34] Therefore, by doping nitrogen atoms into anodic luminescent CDs,[35] it was expected to obtain CDs with stronger anodic ECL emission as well as lower excitation potential, which was promising to hold better applicability to bioanalysis.

In this work, a kind of novel nitrogen doped hydrazide conjugated carbon dots (NHCDs) were prepared through a one-step solvothermal protocol, which presented strong anodic ECL emission at a low excitation potential and applied to rapid detection of living cancer cells. When nitrogen atoms were doped into the graphitic cores of CDs, the highest occupied molecular orbital (HOMO) shifted to the upper energy level, thus the excitation potential was lowered with 0.11 V on the basis of the hydrazide conjugated carbon dots without nitrogen doping (HCDs). Furthermore, as the lower excitation potential reduced the side reactions in the ECL process, the ECL quantum efficiency of NHCDs increased to 2.5-fold. Using the prepared NHCDs as ECL luminophos, a brief biosensor was constructed for sensitive detection of cell-secreted hydrogen peroxide. As shown in Scheme 1, NHCDs could be formed a film on the glassy carbon electrode with the help of chitosan. Then, gold nanoparticles (Au NPs) were fabricated on the film for the immobilization of concanavalin A (Con A), which captured the cells by binding with the glycosyl on the surface of the cells. Differing from healthy somatic cells, the cancer cells secreted more hydrogen peroxide as the active metabolism, which induced stronger ECL emission of NHCDs. By this way, this ECL biosensor could distinguish cancer cells from normal cells with low applied potential in 30 min. The biosensor provided a rapid and sensitive tool to the detection of cancer cells, which presented the application prospects to clinical diagnose of cancer and screening of anticancer drugs. Moreover, this work proposed brief approach to large-scale synthesis of CDs with low excitation potential and strong ECL emission, which were expected to be promising luminophors for in vivo ECL methodology.

EXPERIMENTAL METHOD

Reagents and Materials. Analytical reagents (A.R.) sodium hydroxide, chitosan, *N*,*N*-dimethylformamide (DMF), dichloromethane, hydrazine hydrate, and citric acid (CA) monohydrate were purchased from Chengdu Kelong Chemical Reagent Company (Chengdu, China). Hydrogen peroxide was purchased from Chongqing Chuandong Chemical (group) Co., Ltd. (Chongqing, China). Albumin from bovine serum (BSA) was obtained from J&K Scientific (Beijing, China). Chloroauric acid hexahydrate was purchased from Shanghai Titan Scientific Co., Ltd. (Shanghai, China). Concanavalin A (Con A), Dulbecco's Modified Eagle Medium (DMEM), fetal bovine serum (FBS), and 3-(4,5-dimethylthiazol-2-yl)-2,5-diphenyltetrazolium bromide (MTT) were purchased from Sangon, Inc. (Shanghai, China). Phosphate buffered saline (PBS, pH 7.4, containing NaCl 136.89 mM, KCl 2.67 mM, Na_2HPO_4 8.1 mM, KH_2PO_4 1.76 mM) was used for cell culture and electrolyte solution. Deionized water (18.2 MΩ·cm^{-1}) was used throughout the study. The used living cancer cells (HeLa and MCF-7) were self-cultured. The oral epithelial cells were collected from healthy oral epithelial tissue.

Apparatus. The ECL measurements were performed on MPI-E ECL detection system (Xi'an Remex Electronic Science and Technology Co. Ltd., Xi'an, China). Electrochemical measurement was carried out with a CHI 660C electrochemistry workstation (Shanghai Chenhua Instruments,

DOI: 10.1021/acs.analchem.9b04537
Anal. Chem. 2020, 92, 1379−1385

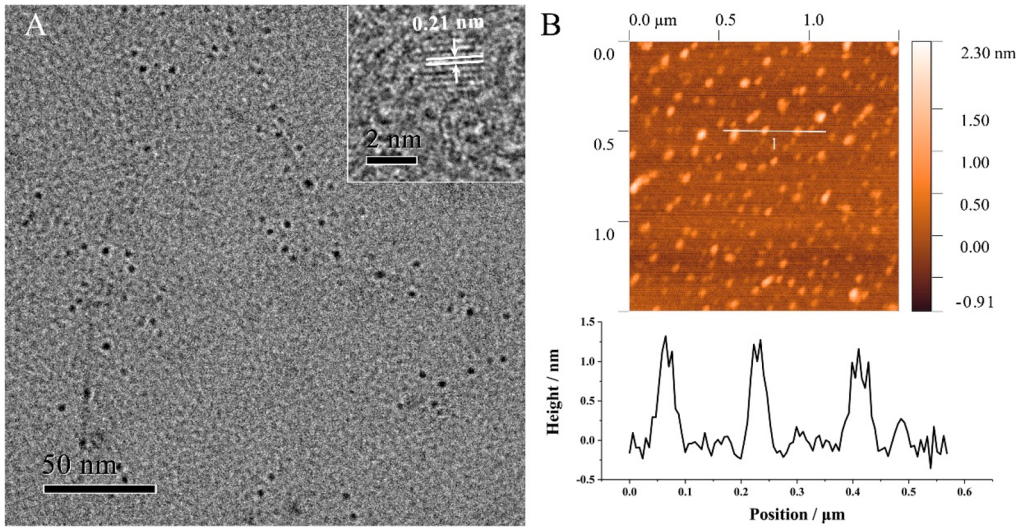

Figure 1. (A) TEM and HRTEM (insert) images of NHCDs; (B) AFM image of NHCDs and the height profile of along the white line.

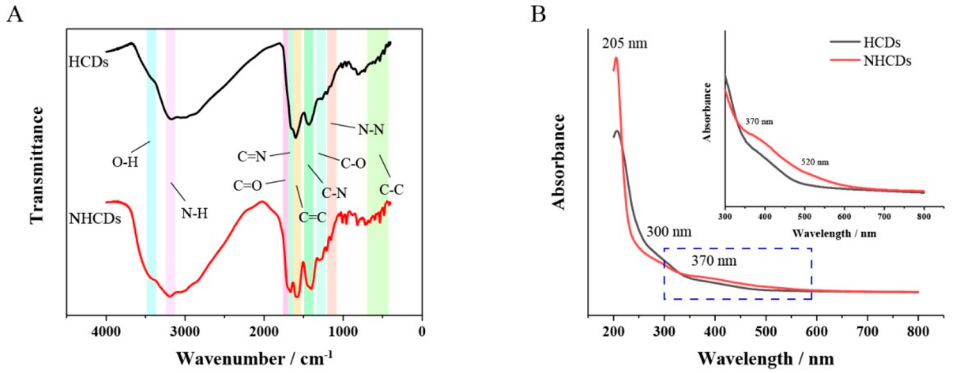

Figure 2. (A) FT-IR spectra and (B) UV−vis absorption spectra of HCDs and NHCDs.

China). A conventional three-electrode system was used for the ECL and electrochemical measurements in the experiment with Ag/AgCl (saturated KCl) as the reference electrode, platinum wire as auxiliary electrode, and modified glassy carbon electrode (GCE, Φ = 4 mm) as working electrode. The transmission electron microscope (TEM) images and high resolution transmission electron microscopy (HRTEM) images were obtained in virtue of a FEI Tecnai G20 (FEI, Hillsboro, Oregon, USA) at an acceleration voltage of 200 kV. X-ray photoelectron spectroscopy (XPS, Thermoelectricity Instruments, USA) were used for elemental analysis. UV−vis absorption spectra were obtained with a UV-2450 UV−vis spectrophotometer (Shimadzu, Tokyo, Japan). Photoluminescence (PL) spectra were measured on FL-7000 spectrophotometer (Hitachi, Tokyo, Japan) at room temperature. A Dimension Icon (Bruker, Santa Barbara, California, USA) atom force microscope (AFM) was employed to measure the thickness of the carbon dots.

Synthesis of NHCDs. Briefly, 2.1 g of citric acid was dissolved in 10 mL of DMF and kept stirring. Then 1.0 mL of hydrazine hydrate was dropwise added into the solution, which turned from colorless solution to ivory gel. The ivory gel was subsequently transferred into a Teflon-lined stainless steel autoclave for solvothermal reaction. After heating treatment at 180 °C for 12 h and cooling down to room temperature, the obtained brown solution was centrifuged (12000 rpm, 10 min) to remove large particle residues. The upper solution was dialyzed (1000 Da) against deionized water and then vacuum-dried at 60 °C. The obtained black powder was stored at 4 °C in an airtight container.

Synthesis of HCDs. As a reference, HCDs were synthesized referring to the synthesis protocol of NHCDs, while water was used as solvent instead of DMF. Then 2.1 g of citric acid were dissolved in 10 mL of water and kept stirring. Then 1.0 mL of hydrazine hydrate was supplied into the solution. The solution was subsequently transferred into a Teflon-lined stainless steel autoclave for hydrothermal reaction. After heating treatment at 180 °C for 12 h and cooling down to room temperature, the obtained brown solution was centrifuged (12000 rpm, 10 min) to remove large particle residues. The upper solution was dialyzed (1000 Da) against deionized water and then vacuum-dried at 60 °C. The obtained black powder was stored at 4 °C in an airtight container.

Fabrication of the ECL Biosensor and H_2O_2 Detection. The glassy carbon electrode (GCE, Φ = 4 mm) was polished to obtain a clean surface according to the reported work.[36] NHCDs (20 μg/mL) and chitosan (1 mg/mL) were dissolved into 1.0% (v/v) acetic acid aqueous solution. Then the mixture solution (10 μL) was cast onto the well-polished GCE surface and dried with nitrogen flow. After forming NHCDs/CS film, the electrode (GCE/NHCDs/CS) was rinsed with 0.1 M sodium hydroxide solution and deionized water successively to remove the excess acetic acid. Subsequently, GCE/NHCDs/

DOI: 10.1021/acs.analchem.9b04537
Anal. Chem. 2020, 92, 1379−1385

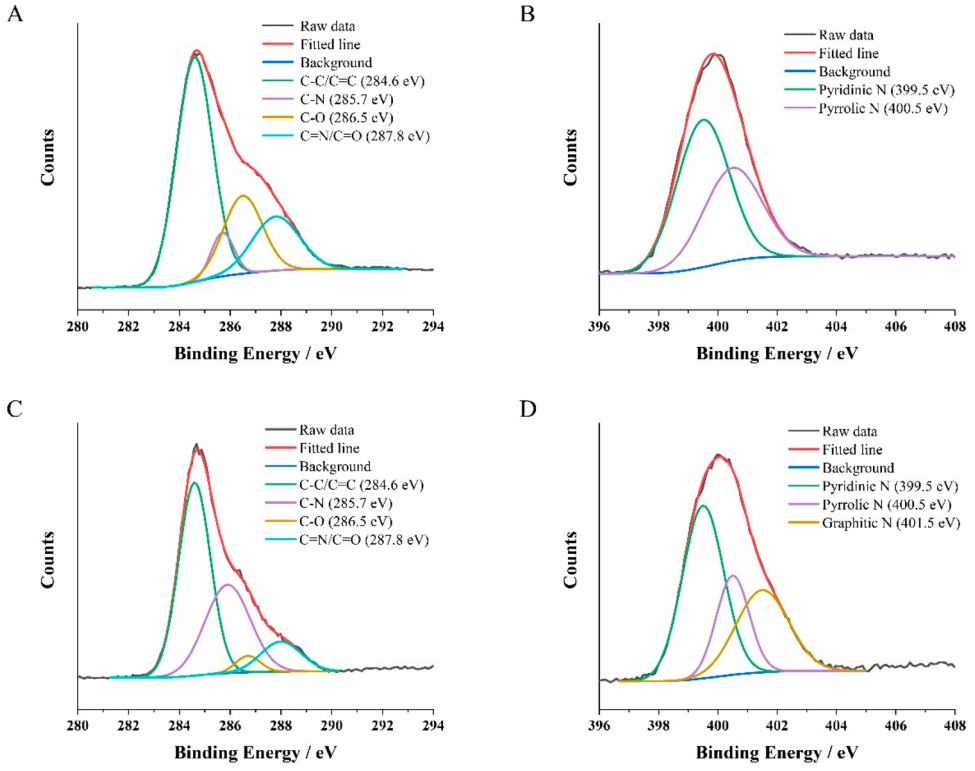

Figure 3. High-resolution C 1s and N 1s XPS spectra for (A,B) HCDs and (C,D) NHCDs.

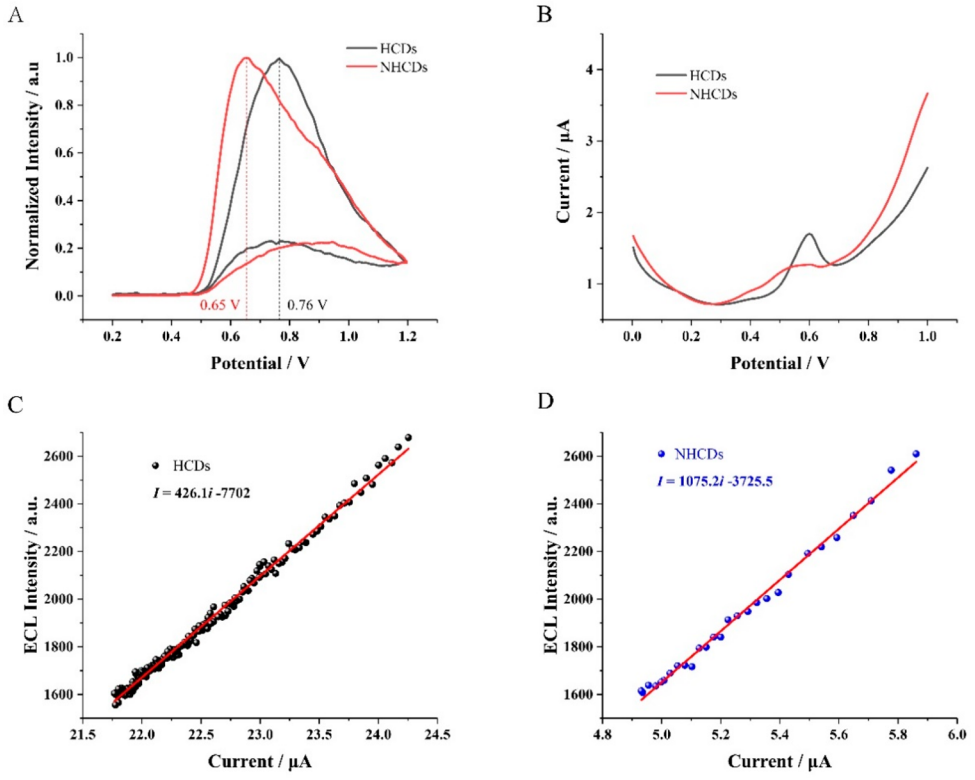

Figure 4. (A) ECL curves of HCDs and NHCDs. (B) DPV curves of HCDs and NHCDs from 0 to 1 V. Calibration curve for the relationship between the ECL intensities and the currents of (C) HCDs and (D) NHCDs.

CS was dried with nitrogen flow to form film again. Then, gold nanoparticles were electrochemically deposited on the electrode at −0.2 V for 15 s (GCE/NHCDs/CS/Au NPs). After being incubated with Con A (1.0 mg/mL) for 2 h and rinsed with PBS, the biosensor was finished fabrication and stored at 4 °C for further use.

ECL Measurement for Cell Detection. For the detection of H_2O_2 secreted by living cells, the cells were incubated on the

DOI: 10.1021/acs.analchem.9b04537
Anal. Chem. 2020, 92, 1379−1385

GCE/NHCDs/CS/Au NPs/Con A surface in an incubator for 30 min for the immobilization of cells. Before measurement, the electrodes with the cells were rinsed with PBS twice to remove the unattached cells. Finally, the ECL intensities were measured by applying the potential from 0.2 to 0.8 V with the scanning rate of 0.1 V/s in PBS.

RESULTS AND DISCUSSION

Morphology Study of NHCDs. Transmission electron microscopy (TEM) and atomic force microscope (AFM) were employed to survey the morphology of NHCDs. As shown in Figure 1A, monodispersed particles were observed in the scope with an average diameter of about 3 nm, manifesting the good dispersity and homogeneity of the prepared NHCDs. High-resolution TEM image presented the morphology of an individual particle, which showed prominent crystal fringes with a spacing of 0.21 nm, implying an at least partially ordered graphene-like structure in NHCDs. AFM image (Figure 1B) showed a thickness of about 1.2 nm for NHCDs, corresponding to the thickness of 2 graphene layers.

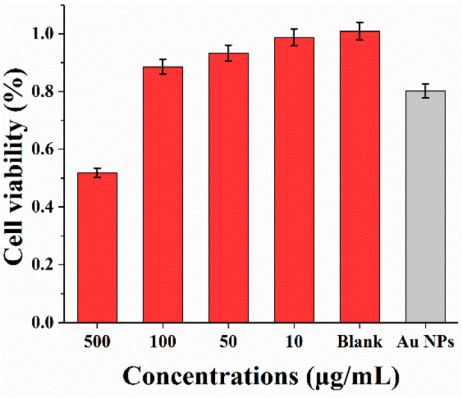

Figure 5. Viability of MCF-7 cells after incubated with different concentrations of NHCDs for 48 h.

Structural Analysis of NHCDs. To investigate the structure of NHCDs, Fourier transform infrared (FT-IR) spectra, UV−vis absorption spectrum, and X-ray photoelectron spectra (XPS) were measured with HCDs as a contrast.

FT-IR was employed to survey the functional groups of the CDs. As shown in Figure 2A, NHCDs exhibited almost identical functional groups with HCDs. FT-IR bands at 3310 and 1645 cm^{-1} were assigned to the N−H and C═O stretching vibrations of amide II, respectively. Moreover, a band contributed to the N−N stretching vibration was observed at 1100 cm^{-1}, confirming the abundant hydrazide groups of both HCDs and NHCDs. The O−H at 3410 cm^{-1} and C−O at 1280 cm^{-1} could be observed in the FT-IR spectra as well, revealing the residual hydroxyl and carboxyl groups that contributed to the water solubility. In addition, the FT-IR bands at 1635, 1597, and 1433 cm^{-1} corresponded to the C═N, C═C, and C−N stretching vibrations, respectively, implying the formation of polyaromatic structures. In spite of the above similarities, the distinct difference in fingerprint region reveals the significant distinctions between HCDs and NHCDs. The specific bands at 480, 535, 600, and 660 cm^{-1} were assigned to the C−C vibrations of the polyaromatic structures. Distinctly, these bands presented much sharper peaks on the spectra of NHCDs than that of HCDs because the doped nitrogen atoms increased the dipole moment of the bonds thereby enhanced the absorption.

UV−vis absorption spectra further depicted the structural similarities and differences of NHCDs from HCDs. As shown in Figure 2B, the UV−vis spectrum of both HCDs and NHCDs showed a typical $\pi-\pi^*$ transition in the region 200−250 nm (assigned to the graphitic cores of CDs) and two $n-\pi^*$ transitions at 300 and 370 nm (assigned to the hydrazide groups conjugated to the graphitic cores). However, another lower energy absorption band could be observed with NHCDs at 520 nm ($n-\pi^*$ transitions), revealing the reduced HOMO−LUMO gap, which was ascribed to the extra p electrons of doped nitrogen atoms to the π-conjugated states.

XPS revealed the structures of HCDs and NHCDs by elucidating the bonding states of carbon and nitrogen in HCDs and NHCDs. The full spectra of both HCDs and NHCDs showed three typical peaks of C 1s (285 eV), N 1s (400 eV), and O 1s (531 eV),[37] which suggested that HCDs and NHCDs contained the same elements (see in Supporting Information, Figure S1). In the high-resolution spectra, the C 1s band of both HCDs and NHCDs could be deconvoluted into similar four peaks, corresponding to C−C/C═C at 284.6 eV, C−N at 285.1 eV, C−O at 286.6 eV, and O═C−O at 288.5 eV, manifesting their similarities in graphitic cores and surficial functional groups (Figure 3A,C). However, distinct difference was observed with the N 1s spectra. As shown in Figure 3B,D, HCDs displayed only two components of pyridinic N (399.5 eV) and pyrrolic N (400.5 eV), which were totally ascribed to the hydrazide groups and their

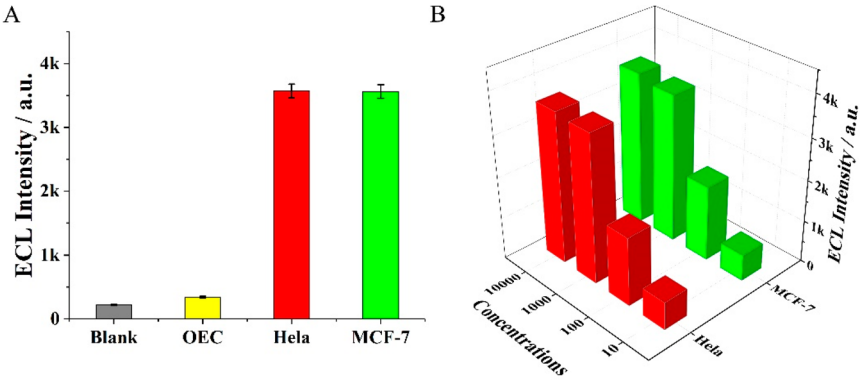

Figure 6. (A) ECL response of the biosensor to different cells (1000 cells in 10 μL). (B) ECL response of the biosensor to Hela and MCF-7 at different concentrations.

DOI: 10.1021/acs.analchem.9b04537
Anal. Chem. 2020, 92, 1379−1385

anions.[35] While NHCDs displayed three components, including pyridinic N (399.5 eV), pyrrolic N (400.5 eV), and graphitic N (401.5 eV), indicating extra nitrogen was doped in the graphitic core of NHCDs, which might be originated from DMF.

The above structural analyses traced out the structure of NHCDs, which was composed of nitrogen doped graphitic core and some suprtrficial functional groups, including hydrazide, hydroxyl, and carboxyl groups.

ECL Properties of NHCDs. The unique ECL properties of NHCDs were demonstrated by comparing the excitation potential and ECL quantum efficiency of NHCDs with those of HCDs. Figure 4A displayed the ECL curve of HCDs and NHCDs, which achieved peak intensity at 0.76 and 0.65 V, respectively, indicating that NHCDs could be excited at lower potential. Moreover, differential pulse voltammetry (DPV) was executed to determine the oxidation potentials of HCDs and NHCDs. As shown in Figure 4B, notable oxidation currents of NHCDs and HCDs were observed at 0.5 and 0.6 V, respectively, which were well corresponding to their ECL excitation potentials. According to the literature,[38] the oxidation peak was corresponding to the energy level of HOMO. Therefore, the lower ECL excitation potential of NHCDs could be ascribed to the upper shift of HOMO induced by nitrogen doping. According to electrochemical investigation (see in Supporting Information, Figure S3), the ECL mechanism of NHCDs was summarized as following:

$$H_2O_2 - e \rightarrow O_2^{\bullet -} + 2H^+ \quad (0.28\ \text{V vs Ag/AgCl})$$

$$NHCDs - e \rightarrow NHCDs^+ \quad (0.65\ \text{V vs Ag/AgCl})$$

$$NHCDs^+ \rightarrow NHCDs^{\bullet} + H^+$$

$$O_2^{\bullet -} + NHCDs^{\bullet} \rightarrow NHCDs^* + N_2$$

$$NHCDs^* \rightarrow NHCDs + h\nu$$

ECL quantum efficiency is a recognized parameter to quantify the ECL performance. Herein, potentiostatic method was employed to excite the ECL of HCDs (0.76 V) and NHCDs (0.65 V). The ECL quantum efficiencies could be calculated according to the quantitative relation between ECL intensity and current. As shown in Figure 4C,D, the ECL intensities of HCDs and NHCDs exhibited well linear response to currents, respectively. According to the equation:[20,36]

$$\varnothing_x = \varnothing_{st}\left(\frac{\int_0^t I\,dt}{\int_0^t i\,dt}\right)_x \Bigg/ \left(\frac{\int_0^t I\,dt}{\int_0^t i\,dt}\right)_{st} \quad (1)$$

the ECL intensity was proportional to the Faradaic current in a given ECL system, which was verified by the experimental results. The quantitative relation between ECL intensity and current could be summarized as following equations:

$$I_{HCDs} = k_{HCDs} i_F = k_{HCDs}(i - i_n) = 426.1i - 7702 \quad (2)$$

$$I_{NHCDs} = k_{NHCDs} i_F = k_{NHCDs}(i - i_n) = 1075.2i - 3725.5 \quad (3)$$

Here, I, i_F, i_n, t, and k stand for the ECL intensity, Faradaic current, non-Faradaic current, time, and the slope of the linear response curve, respectively. Therefore, the quotient of $\varnothing_{HCDs}$ and $\varnothing_{NHCDs}$ (Q) could be calculated as the following equation:

$$Q = \frac{\varnothing_{NHCDs}}{\varnothing_{HCDs}} = \left(\frac{\int_0^t I\,dt}{\int_0^t i_F\,dt}\right)_{NHCDs} \Bigg/ \left(\frac{\int_0^t I\,dt}{\int_0^t i_F\,dt}\right)_{HCDs}$$
$$= \left(\frac{\int_0^t k i_F\,dt}{\int_0^t i_F\,dt}\right)_{NHCDs} \Bigg/ \left(\frac{\int_0^t k i_F\,dt}{\int_0^t i_F\,dt}\right)_{HCDs}$$
$$= \frac{k_{NHCDs}}{k_{HCDs}} = \frac{1075.2}{426.1} = 2.5 \quad (4)$$

The result showed that NHCDs exhibited 2.5-fold ECL quantum efficiency of HCDs. However, HCDs and NHCDs showed little distinction in photoluminescence spectra, ECL spectra (see in Supporting Information, Figure S4). Meanwhile, the photoluminescence quantum yields of HCDs and NHCDs were 10.7% and 11.5%, indicating that the emission efficiency of excited species were approximate. Therefore, higher ECL quantum efficiency should be ascribed to the higher electron transfer efficiency in the ECL process of NHCDs because the low excitation potential significantly reduced the side reactions, for instance, the electrochemical oxidation of glassy carbon by $O_2^{\bullet -}$.[39]

Cytotoxicity of the NHCDs. Cytotoxicity was an important indicator to judge the biocompatibility of the CDs in cell experiments. Herein, standard MTT assays were performed with MCF-7 cells to evaluate the cytotoxicity of the obtained NHCDs. Figure 5 shows the viability of MCF-7 cells after the incubation with NHCDs samples at different concentrations (10, 50, 100, and 500 μg/mL). Over 85% of MCF-7 cells are still alive after incubation with 100 μg/mL of NHCDs for 48 h, which is approximate to the level of 1.0 μg/mL Au NPs, manifesting the low cytotoxicity of the NHCDs toward living cells.

Detection of H_2O_2 Released from Living Cells. To evaluate the application potential of the NHCDs to cell analysis, a brief biosensor was fabricated for the detection of H_2O_2 released from living cells. For comparison, oral epithelial cells (OEC), HeLa, and MCF-7 were tested with the biosensor, respectively. Figure 6A displayed the ECL signal of the biosensor detected with different cells. Apparently, only a weak ECL signal could be detected with the oral epithelial cells, as highly differentiated cells just maintained a basic metabolism and released little H_2O_2. In contrast, strong ECL signals were observed with Hela and MCF-7, respectively, which was ascribed to the high metabolism of cancer cells, releasing abundant H_2O_2. The results indicated that the NHCDs and biosensor were qualified in the analysis of cell activity. Furthermore, ECL response of the biosensor was measured with HeLa and MCF-7 at different concentrations. As shown in Figure 6B, notable increase was observed with the ECL intensity response to the increased concentration of Hela and MCF-7, respectively, manifesting the potential of the biosensor for quantification of cancer cells.

CONCLUSION

In summary, this work proposed a facile solvothermal approach for the preparation of hydrazide conjugated CDs with nitrogen doped graphitic cores. Specifically, comparing to the hydrazide conjugated CDs with nondoped graphitic cores, the as-prepared CDs exhibited higher ECL quantum efficiency and could be excited with lower potential. Researches showed that nitrogen doping in the graphitic cores increased the HOMO

DOI: 10.1021/acs.analchem.9b04537
Anal. Chem. 2020, 92, 1379−1385

energy level of CDs, thus lowering the oxidation potential, resulting in the low excitation potential. Meanwhile, the low excitation potential reduced the side reactions in the ECL process thereby improved the ECL quantum efficiency. On the basis of the high performance NHCDs, a ECL biosensor was fabricated to rapidly distinguish cancer cells from normal cells. This work proposed not only an effective method for cancer cell detection but also a promising ECL luminophor for bioanalysis. Moreover, the nitrogen doping strategy inspired a feasible way to further improve the ECL performance of CDs.

■ ASSOCIATED CONTENT

Supporting Information

The Supporting Information is available free of charge at https://pubs.acs.org/doi/10.1021/acs.analchem.9b04537.

XPS spectra in full region, ECL spectra, photoluminescence spectra, and standard H_2O_2 tests (PDF)

■ AUTHOR INFORMATION

Corresponding Authors

*R. Yuan: phone, +86 23 68252277; fax, +86 23 68253172; E-mail, yuanruo@swu.edu.cn.

*Y. Q. Chai: E-mail, yqchai@swu.edu.cn.

ORCID

Wenbin Liang: 0000-0002-9086-4974

Ying Zhuo: 0000-0002-4491-1186

Yaqin Chai: 0000-0003-4392-9592

Ruo Yuan: 0000-0003-3664-6236

Notes

The authors declare no competing financial interest.

■ ACKNOWLEDGMENTS

This research was financially supported by the NNSF of China (21575116, 21974108, 21675129, 21775124), China.

■ REFERENCES

(1) Peng, H. P.; Huang, Z. N.; Sheng, Y. L.; Zhang, X. P.; Deng, H. H.; Chen, W.; Liu, J. W. *Angew. Chem., Int. Ed.* **2019**, *58*, 11691−11694.

(2) Liu, J. L.; Zhang, J. Q.; Tang, Z. L.; Zhuo, Y.; Chai, Y. Q.; Yuan, R. *Chem. Sci.* **2019**, *10*, 4497−4501.

(3) Zhang, J. J.; Arbault, S.; Sojic, N.; Jiang, D. C. *Annu. Rev. Anal. Chem.* **2019**, *12*, 275−295.

(4) Al-Kutubi, H.; Voci, S.; Rassaei, L.; Sojic, N.; Mathwig, K. *Chem. Sci.* **2018**, *9*, 8946−8950.

(5) Voci, S.; Goudeau, B.; Valenti, G.; Lesch, A.; Jovic, M.; Rapino, S.; Paolucci, F.; Arbault, S.; Sojic, N. *J. Am. Chem. Soc.* **2018**, *140*, 14753−14760.

(6) Chen, A. Y.; Ma, S. Y.; Zhuo, Y.; Chai, Y. Q.; Yuan, R. *Anal. Chem.* **2016**, *88*, 3203−3210.

(7) Yang, L.; Fan, D. W.; Zhang, Y.; Ding, C. F.; Wu, D.; Wei, Q.; Ju, H. X. *Anal. Chem.* **2019**, *91*, 7145−7152.

(8) Zhao, G. H.; Wang, Y. G.; Li, X. J.; Yue, Q.; Dong, X.; Du, B.; Cao, W.; Wei, Q. *Anal. Chem.* **2019**, *91*, 1989−1996.

(9) Liang, W. B.; Yang, M. Z.; Zhuo, Y.; Zheng, Y. N.; Xiong, C. Y.; Chai, Y. Q.; Yuan, R. *Chem. Sci.* **2016**, *7*, 7094−7100.

(10) Ge, J. J.; Zhao, Y.; Li, C. L.; Jie, G. F. *Anal. Chem.* **2019**, *91*, 3546−3554.

(11) Huo, X. L.; Zhang, N.; Yang, H.; Xu, J. J.; Chen, H. Y. *Anal. Chem.* **2018**, *90*, 13723−13728.

(12) Liu, Z. Y.; Qi, W. J.; Xu, G. B. *Chem. Soc. Rev.* **2015**, *44*, 3117−3142.

(13) Li, L. L.; Chen, Y.; Zhu, J. J. *Anal. Chem.* **2017**, *89*, 358−371.

(14) Li, S. J.; Liu, Y.; Ma, Q. *TrAC, Trends Anal. Chem.* **2019**, *110*, 277−292.

(15) Zhang, J. J.; Jin, R.; Jiang, D. C.; Chen, H. Y. *J. Am. Chem. Soc.* **2019**, *141*, 10294−10299.

(16) Liu, G.; Ma, C.; Jin, B. K.; Chen, Z. X.; Zhu, J. J. *Anal. Chem.* **2018**, *90*, 4801−4806.

(17) Liu, Y.; Chen, X. Q.; Wang, M. K.; Ma, Q. *Green Chem.* **2018**, *20*, 5520−5527.

(18) Zhao, Z. N.; Zhang, X.; Li, C. E.; Chen, T. F. *Biomaterials* **2019**, *192*, 579−589.

(19) Notaro, A.; Gasser, G. *Chem. Soc. Rev.* **2017**, *46*, 7317−7337.

(20) Wang, F.; Lin, J.; Zhao, T. B.; Hu, D. D.; Wu, T.; Liu, Y. *J. Am. Chem. Soc.* **2016**, *138*, 7718−7724.

(21) Liu, S. L.; Zhang, Q. H.; Zhang, L.; Gu, L.; Zou, G. Z.; Bao, J. C.; Dai, Z. H. *J. Am. Chem. Soc.* **2016**, *138*, 1154−1157.

(22) Bhattacharyya, S.; Ehrat, F.; Urban, P.; Teves, R.; Wyrwich, R.; Doblinger, M.; Feldmann, J.; Urban, A. S.; Stolarczyk, J. K. *Nat. Commun.* **2017**, *8*, 1401.

(23) Li, Q. J.; Zhou, M.; Yang, M. Y.; Yang, Q. F.; Zhang, Z. X.; Shi, J. *Nat. Commun.* **2018**, *9*, 734.

(24) Lu, S. Y.; Xiao, G. J.; Sui, L. Z.; Feng, T. L.; Yong, X.; Zhu, S. J.; Li, B. J.; Liu, Z. Y.; Zou, B.; Jin, M. X.; Tse, J. S.; Yan, H.; Yang, B. *Angew. Chem., Int. Ed.* **2017**, *56*, 6187−6191.

(25) Zheng, L. Y.; Chi, Y. W.; Dong, Y. Q.; Lin, J. P.; Wang, B. B. *J. Am. Chem. Soc.* **2009**, *131*, 4564.

(26) Carrara, S.; Arcudi, F.; Prato, M.; De Cola, L. *Angew. Chem., Int. Ed.* **2017**, *56*, 4757−4761.

(27) Chen, Y.; Zhou, S. W.; Li, L. L.; Zhu, J. J. *Nano Today* **2017**, *12*, 98−115.

(28) Cai, X. L.; Zheng, B.; Zhou, Y.; Younis, M. R.; Wang, F. B.; Zhang, W. M.; Zhou, Y. G.; Xia, X. H. *Chem. Sci.* **2018**, *9*, 6080−6084.

(29) Zhang, H.; Zhang, X. W.; Dong, S. J. *Anal. Chem.* **2015**, *87*, 11167−11170.

(30) Zhang, R. Z.; Adsetts, J. R.; Nie, Y. T.; Sun, X. H.; Ding, Z. F. *Carbon* **2018**, *129*, 45−53.

(31) Liu, G.; Ma, C.; Jin, B. K.; Chen, Z. X.; Cheng, F. L.; Zhu, J. J. *Anal. Chem.* **2019**, *91*, 3021−3026.

(32) Niu, W. J.; Zhu, R. H.; Cosnier, S.; Zhang, X. J.; Shan, D. *Anal. Chem.* **2015**, *87*, 11150−11156.

(33) Liu, Z. Q.; Cheng, H.; Li, N.; Ma, T. Y.; Su, Y. Z. *Adv. Mater.* **2016**, *28*, 3777−3784.

(34) Wang, Y.; Shao, Y. Y.; Matson, D. W.; Li, J. H.; Lin, Y. H. *ACS Nano* **2010**, *4*, 1790−1798.

(35) Dong, Y. Q.; Dai, R. P.; Dong, T. Q.; Chi, Y. W.; Chen, G. N. *Nanoscale* **2014**, *6*, 11240−11245.

(36) Chen, A. Y.; Zhao, M.; Zhuo, Y.; Chai, Y. Q.; Yuan, R. *Anal. Chem.* **2017**, *89*, 9232−9238.

(37) Ding, H.; Wei, J. S.; Zhong, N.; Gao, Q. Y.; Xiong, H. M. *Langmuir* **2017**, *33*, 12635−12642.

(38) Chen, S.; Ma, H.; Padelford, J. W.; Qinchen, W.; Yu, W.; Wang, S.; Zhu, M.; Wang, G. *J. Am. Chem. Soc.* **2019**, *141*, 9603−9609.

(39) Zhou, M.; Zhai, Y. M.; Dong, S. J. *Anal. Chem.* **2009**, *81*, 5603−5613.

DOI: 10.1021/acs.analchem.9b04537
Anal. Chem. 2020, 92, 1379−1385